Atmosphere **2012**, *3*, 1-x manuscripts; doi:10.3390/atmos30x000x

OPEN ACCESS

atmosphere

ISSN 2073-4433

www.mdpi.com/journal/atmosphere

Article

Atmospheric aerosol distributions and cloud properties using multi-wavelength Raman lidar measurements

Sachin J. Verghese [1] and C. Russell Philbrick [2,*]

[1] Ansys Inc., 275 Technology Dr. Canonsburg PA 15317 USA; E-Mail: sachin.verghese@ansys.com

[2] NC State University, Physics Dept. Raleigh NC 27695-8202 USA; E-Mail: philbrick@ncsu.edu

***** Author to whom correspondence should be addressed; E-Mail: philbrick@ncsu.edu; Tel.: +001-919-513-7174; Fax: +001-919-515-6538.

Received: / Accepted: / Published:

Abstract: Improved measurements of atmospheric aerosol properties are essential for a better understanding of the roles of aerosols in processes that modify the Earth's radiation budget. Raman lidars have been used for a number of years to measure the profiles of N_2, O_2, H_2O, O_3, optical extinction, and temperature using the vibrational and rotational Raman scatter signals. Measurements obtained during several field campaigns have provided datasets for investigating aerosol and cloud properties. The extinction profiles at several wavelengths are used to observe changes in the aerosol sizes in the accumulation mode range. Models based on Mie scattering calculations are compared with measurements of multi-wavelength extinction to investigate changes in the size of particles as clouds develop and dissipate. We demonstrate the capability of this technique using the multi-wavelength extinction ratios to observe changes in particle sizes in the range 50 nm to 1.0 μm. An example is used to demonstrate changes in the size of cloud particles observed during formation and dissipation stages of cloud evolution using multi-wavelength aerosol extinction profiles. We also examine the relationships that exist as particle sizes increase or decrease by comparing multi-wavelength extinction coefficients with changes in relative humidity.

Keywords: aerosols; clouds; Raman lidar; optical extinction profiles; cloud growth and dissipation

---

1. Introduction

Atmospheric aerosols are generated from various natural and anthropogenic sources and include all liquid and solid particles, except pure water, that exist in the atmosphere under normal conditions [1]. The largest anthropogenic increases in aerosol concentrations are due to the direct emission of elemental carbon and organic aerosols from incomplete combustion of carbonaceous fuels, and the nucleation associated with primary emissions of sulfate, ammonia, nitrate, and condensable organic species from industrial activities, power generation, transportation, biomass burning, and fertilizers [2].

The distribution of aerosols in the atmosphere influences Earth's climate because of scattering and absorption of radiation by particles. Aerosols and clouds play a major role in determining what fraction of the solar radiation incident at the top of the atmosphere reaches the Earth's surface and also regulate the transfer of infrared radiation back to space. The propagation of shortwave and long-wave electromagnetic radiation through the atmosphere is determined by the spatial distribution, concentration and size of aerosols and cloud particles, and hence a detailed understanding of these layers has become important. Aerosols assert a direct effect by scattering and absorbing radiation. They also assert an indirect effect by influencing the formation, microphysical properties, and lifetime of cloud structures. The indirect effect, resulting from changes in cloud albedo, microphysical properties, and increased lifetimes, is not yet fully understood, but is thought to exert a negative radiative forcing on the climate system [3-5]. The concern for models that help us study the indirect effects of aerosols is the relationship between sub-cloud aerosol populations and the processes of cloud droplet formation upon them. The detailed representation of clouds in general circulation models has thus become a major problem for scientists as it is obviously impossible to simulate and predict Earth's climate accurately without such knowledge. Aerosols also impact human health because they provide a way of concentrating the chemical species resulting from air pollution into the lungs. Recent assessments conclude that the largest uncertainties in the impact of human activity on global mean radiative forcing are due to the lack of understanding of how pollution influences cloud patterns and the attributes of individual clouds [2].

The scientific challenges of developing better techniques to monitor and model our atmosphere gained increased priority due to the growing number of questions concerning our changing environment and its impact on human life. Part of the challenge lies in accurately measuring the various formation processes of atmospheric aerosols because of the influence of various minor species on the growth rate, hygroscopic properties, and nucleation processes. In-situ methods of atmospheric sensing, such as those using aircraft and balloons, require constant human involvement, can only operate for several hours at a time, are expensive to maintain, and frequently need to be replaced. Satellite remote sensing provides an important platform for describing large-scale features distributed over global scales, but these systems are extremely expensive, and are too limited in vertical and temporal resolution to study the processes governing aerosol formation. Ground-based lidar techniques have been used to measure aerosol optical parameters and offer several advantages over other measurement techniques. Lidar instruments have the ability to provide good spatial resolution and high temporal resolution at a specific location. Lidar determinations of aerosol size distributions and other properties have been investigated by several research groups, but results have been mostly limited to theory and simulations. Experimental data to demonstrate the retrieval of size distributions are limited

because of the difficulty in analyzing data using inversion techniques, and the range of wavelengths needed to perform an adequate inversion analysis [6]. Advanced techniques using multi-wavelength Raman lidar became extremely important because they provide a key to obtaining these data for a wide range of atmospheric parameters [7-11].

Raman lidar is one of the best tools for describing the aerosol distributions in time and space while studying aerosol and cloud properties. The visible and ultraviolet laser wavelengths typically used for lidar are useful for characterizing particles in the 0.1 to 1 μm range, which also corresponds to the important size range of condensation nuclei and accumulation mode particles; therefore we can derive important information regarding the variations in particle sizes in the regions of formation and dissipation of clouds.

Raman lidar profiles of the primary molecular species are used to profile the atmospheric optical extinction due to aerosols, plumes and clouds. The gradient of the vertical profiles of the primary molecular constituents are reasonably well known from a hydrostatic calculation, which uses a temperature profile from a recent nearby sounding, an appropriate meteorological model data product, or a measured rotational Raman temperature profile. Differences in the gradient of the measured N_2 or O_2 Raman molecular profile from the expected density scale height are used to determine the aerosol optical extinction profile. The measured Raman lidar extinction profile includes the extinction due to aerosol scattering at the transmit wavelength and at the Raman shifted wavelength. The extinction of aerosol scattering at the transmitted and received wavelengths can be ascribed to an intermediate wavelength because of the relatively smooth wavelength dependence; the molecular scatter at each wavelength depends on $1/\lambda^4$. The ratio of the visible and the ultraviolet extinction profiles contains important information on the changes in the relative size of particles in the accumulation mode; thus, we use the multi-wavelength extinction ratios to observe variations as a function of time and altitude.

2. LAPS Raman Lidar Instrument

The Lidar Atmospheric Profile Sensor (LAPS) instrument was built for the U.S Navy by the staff and graduate students in the Lidar Laboratory, Applied Research Laboratory and the Electrical Engineering Department at Penn State University (PSU). LAPS is the fifth generation of Raman lidar instruments designed and fabricated by our research group since the mid-1970's. The LAPS instrument uses an Nd:YAG laser to transmit fundamental and harmonic wavelengths (1064, 532, 355 and 266 nm) to select Raman scatter lines for simultaneous measurements of profiles of water vapor, temperature, ozone and optical extinction with a 75 m range resolution [7]. Measurements of the atmospheric properties are obtained from the range-resolved intensity of the return signals at the transmitted wavelengths and at several Raman shifted wavelengths. Initial testing was for the U.S. Navy onboard the USNS SUMNER during September and October 1996 in the Gulf of Mexico and Atlantic Ocean. Since that time it has been used for a number of research investigations, and has provided a large dataset that is used for studies of aerosols, cloud properties and air pollution. PSU's LAPS Raman lidar is a weather sealed and rugged instrument that was designed for semi-automatic operation to enable data collection in virtually any environment.

The Raman scattering technique has many advantages in obtaining quantitative measurements of several chemical and physical properties simultaneously. Raman scatter signals are used to profile the

signal of a trace constituent and quantify its concentration relative to a major constituent, such as molecular nitrogen [12]. The LAPS instrument uses the vibrational Raman scattered signals to measure water vapor, ozone and optical extinction, and uses the rotational Raman scatter signals to measure temperature and optical extinction. Several different operating modes can be selected, but the instrument typically collect the backscatter signals, rotational Raman backscatter signals at 528 nm and 530 nm, and vibrational Raman backscatter signals at 607, 660, 277, 284 and 295 nm. The 607 and 660 nm signals are the 1st Stokes vibrational Raman shifts from the N_2 and H_2O molecules excited by the second harmonic (532 nm) of the Nd:YAG laser. The 277 nm, 284 nm and 295 nm signals correspond to the vibrational Raman shifts from the O_2, N_2, and H_2O molecules in the atmosphere excited by the fourth harmonic (266 nm) of the Nd:YAG laser. The LAPS instrument measures the water vapor concentration by forming the ratio of the Raman signals from water vapor and nitrogen. Profiles of water vapor can be obtained during the day and night using the 295/284 ratio and at night using 660/607 ratio of the ultraviolet and visible wavelengths [7, 8, 13, 14].

Optical extinction, which is a measure of the total attenuation of a laser beam due to scattering and absorption in the atmosphere, is obtained directly from the slope of the molecular profiles compared to the expected signal gradient based on the hydrostatic equation and the $1/r^2$ geometry. The LAPS instrument measures the optical extinction profiles from the gradients in each of the measured molecular profiles, 607 nm, 530 nm and 284 nm. The 530 nm signal includes a narrow band of rotational Raman lines, which are primarily used in the temperature profile determination. The narrow band of N_2 and O_2 rotational lines selected near the peak of the rotational band is relatively constant in amplitude, and we have found that the magnitude of the 530 nm signal also provides an excellent measurement of the optical extinction. The magnitude of this signal can also be used to determine the magnitude of the $\Delta J = 0$ Cabannas line; thereby allowing a direct measurement of the lidar ratio. At these wavelengths the extinction is primarily from optical scattering due to aerosols, combined with a relatively small and known contribution due to extinction by molecular scattering. The extinction coefficient can be derived directly from the Raman lidar equation [15], which can be written as,

$$P(\lambda_R, z) = P_T(\lambda_T)\xi_T(\lambda_T)\xi_R(\lambda_R)\frac{c\tau}{2}\frac{A}{z^2}\beta(\lambda_T, \lambda_R)\exp\left[-\int_0^z [\alpha(\lambda_T, z') + \alpha(\lambda_R, z')]dz'\right] \quad (1)$$

where z is the altitude of the scattering volume element, λ_T is the wavelength transmitted, λ_R is the wavelength received, $P_T(\lambda_T)$ is the power transmitted at wavelength λ_T, $\xi_T(\lambda_T)$ is the net optical efficiency of all transmitting devices at wavelength λ_T, $\xi_R(\lambda_R)$ is the net optical efficiency of each receiving device at wavelength λ_R, c is the speed of light, τ is the time duration of the laser pulse, A is the area of the receiving telescope, $\beta(\lambda_T,\lambda_R)$ is the back scattering cross section of the volume element for the laser wavelength λ_T at Raman shifted wavelength λ_R, and $\alpha(\lambda,z')$ is the extinction coefficient at wavelength λ at range z'. The extinction coefficients in Eq. (1) can be written as,

$$\alpha(\lambda_T,z)+\alpha(\lambda_R,z)=\alpha_{\lambda_T}^{mol\text{-}sca}(z)+\alpha_{\lambda_T}^{aer\text{-}sca}(z)+\alpha_{\lambda_R}^{mol\text{-}sca}(z)+\alpha_{\lambda_R}^{aer\text{-}sca}(z)+\alpha_{\lambda_T}^{abs}(z)+\alpha_{\lambda_R}^{abs}(z), \quad (2)$$

where $\alpha_\lambda^{mol-sca}(z)$ and $\alpha_\lambda^{aer-sca}(z)$ are the extinction coefficients due to molecular and aerosol scattering at the transmit and receive wavelengths, and α_λ^{abs} are the molecular and aerosol extinction

coefficients due to optical absorption. The molecular scattering contribution to the extinction can be easily calculated from temperature profile measurements or models. The temperature profile is obtained from the LAPS profiles of the rotational Raman nighttime measurements. The selected visible wavelengths do not correspond to any significant molecular absorption features in the atmosphere, but the ultraviolet wavelengths do experience absorption due to ozone. The extinction at visible wavelengths is primarily due to aerosol and molecular scatter contributions. The aerosol extinction coefficient at the visible wavelengths can be expressed by rewriting Equation (1) as,

$$\alpha_{\lambda_R}^{aer} = \frac{\frac{d}{dz}\left[\ln \frac{N(z)}{P(z)z^2}\right] - \alpha_{\lambda_T}^{mol}(z) - \alpha_{\lambda_R}^{mol}(z)}{1 + \frac{\lambda_T}{\lambda_R}} \quad (3)$$

At the UV wavelengths, between 200 nm and 300 nm, the absorption due to ozone is significant. Since the absorption cross-section for ozone in the Hartley band is well known (<1%), and the ozone concentration is measured from the departure of the measured O_2/N_2 ratio from its expected constant value, it is possible to determine the ultraviolet extinction due to aerosols [17,18]. For the UV wavelengths the extinction equation includes the compensation for the ozone absorption as,

$$\alpha_{\lambda_R}^{aer} = \frac{\frac{d}{dz}\left[\ln \frac{N(z)}{P(z)z^2}\right] - \alpha_{\lambda_T}^{mol}(z) - \alpha_{\lambda_R}^{mol}(z) - \alpha_{\lambda_T}^{Abs}(z) - \alpha_{\lambda_R}^{Abs}(z)}{1 + \frac{\lambda_T}{\lambda_R}} \quad (4)$$

The LAPS instrument measures the water vapor mixing ratio by taking the ratio of the signals from the 1st Stokes vibrational Raman shifts for water vapor and nitrogen. Profiles of water vapor can be obtained during the day (295/284) and the night (660/607) with the ultraviolet and visible laser wavelengths [13,14]. The water vapor mixing ratio is expressed by taking the ratio of its number density to the number density of ambient air and multiplying by a calibration constant. The equation to obtain vertical profiles of water vapor at visible wavelengths is,

$$W(z) = K_{cal} \frac{S_{H2O}(z)}{S_{N2}(z)} \quad (5)$$

where, S_{H2O} is the received signal from the vibrational Raman shift of H_2O at 660 nm, S_{N2} is the received signal from the vibrational Raman shift of N_2 at 607 nm, and K_{cal} is a calibration constant. The calibration constant, K_{cal}, may be obtained by fitting the ratio of the return signals of H_2O and N_2 with the data obtained from a radiosonde balloon for water vapor profile at the same time. We are taking the ratio of the two signals from the same transmitted wavelength, therefore most of the terms in the lidar equation cancel providing a simpler equation [16]. LAPS obtains daytime measurements by operating in the 'solar blind' spectral interval, between 230 and 300 nm, where stratospheric ozone absorbs the incoming radiation and limits the strong day sky background radiance. Since some of the transmitted radiation is absorbed by tropospheric ozone, correction for ozone absorption is necessary.

3. Discussion and Results

The LAPS lidar has a distinct advantage in being able to measure optical extinction at different wavelengths, and we use the extinction measurements to infer particle size variations by taking ratios of the extinction coefficients measured at the different wavelengths. The aerosol extinction depends on both size and number density of the scattering particles. Changes in the density of a particular size aerosol lead to a proportional response. Figure 1(a) shows a model calculation for a 532 nm laser scattering cross-section from water aerosols with the r^6 dependence for particle size that is expected for particles much smaller than the scattering wavelength, the r^2 dependence observed for larger particles, and the resonance region between occurs for transparent dielectric particles with radius near the scale size of the scattering wavelength [19]. Figure 1(b) shows the ratios of the extinction coefficients for wavelength ratios, 530 nm/284 nm, 607 nm/284 nm and 607 nm/530 nm. These plots are generated from Mie calculations, assuming only spherical particles, using the BHMIE code [20]. The ratios of the extinction coefficients show that when the particle size is small compared to wavelength, the scattered intensity is inversely proportional to the fourth power of the wavelength, while the scatter cross-section increases as the sixth power of the particle radius. For accumulation mode particles, where the size range is between 0.05 μm and 1 μm, the ratios of the extinction coefficients are size dependent and structured as a function of size. For coarse mode particles the ratios lose their size dependence and approach unity (for optical wavelengths in the visible spectrum).

Figure 1. (a) Scattering cross-section calculated for water aerosols n=1.38 illuminated with a 532 nm laser (figure from [19]) using the BHMIE code [20]. Reproduced with permission from T.D. Stevens, Dissertation Penn State University; published by [publisher], [year].' at the end of the caption of the Table, Figure or Scheme. **(b)** Ratios of extinction coefficients as a function of particle size calculated using Mie calculations for three wavelengths where optical extinction values are obtained with the LAPS instrument.

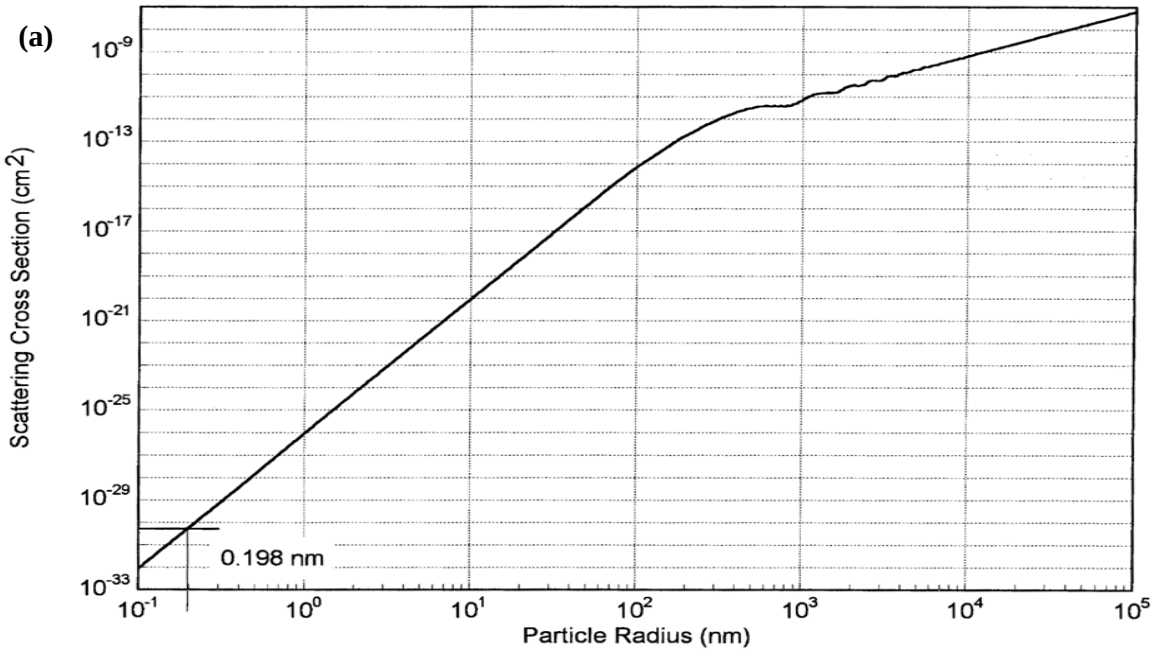

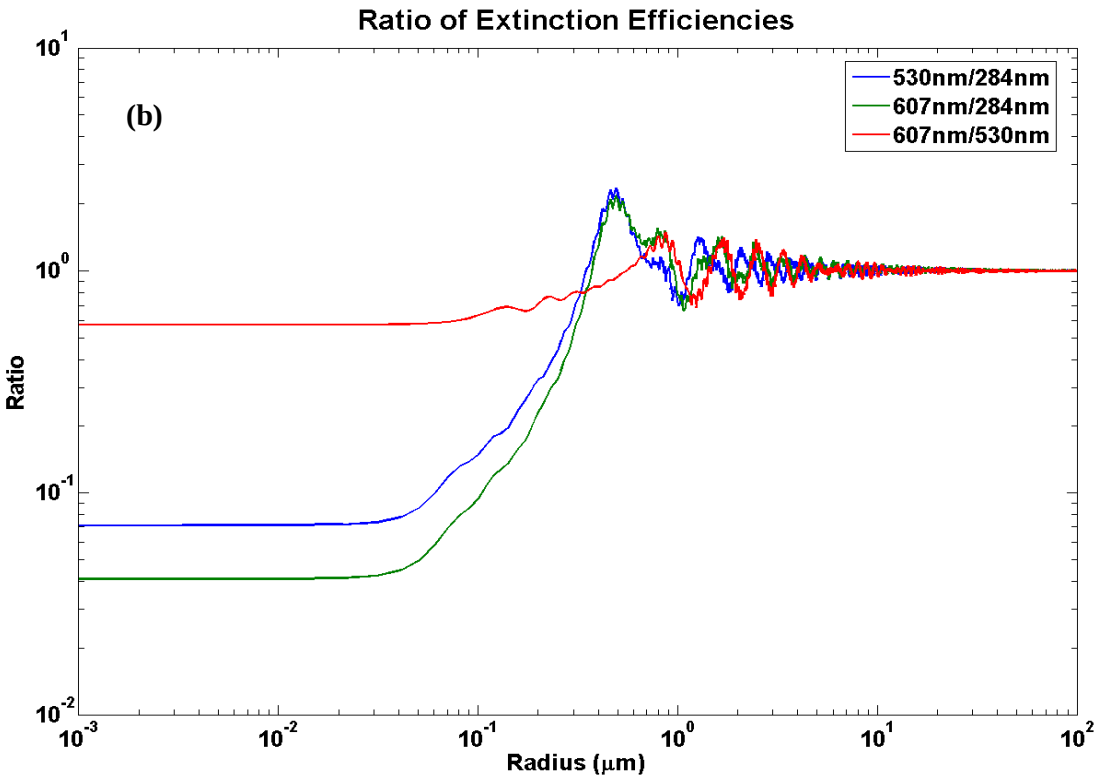

Figure 2 shows an example of the optical extinction measurements made at the three wavelengths during the SCOS97 measurement program [21]. The plots relate to the calculations shown in Figure 1. The vertical profiles show the variations of extinction with altitude. The data obtained have been integrated over a 60 minute period and plotted as a function of altitude. By comparing these data with the model calculations we observe that a large number of aerosol particles (typical size on the order of 0.5 μm) apear to dominate in the lower atmosphere, from the surface near 1.2 km up to about 1.7 km. The UV and visible extinction coefficients imply the presence of accumulation mode particles with size distribution peaked near the mid-wavelengths of visible light. At altitudes between 1.7 km and 4 km, the ultraviolet extinction is much greater than the visible extinction (approximately a factor of 4 or 5) and this suggests a distribution of smaller particles in this region (a ratio of a factor of 12 would imply that the particles are small, probably dominated by sizes less than 50 nm), however the number density of the small particles must be large to result in the high extinction values measured. At higher altitude, we also observe two layers with no significant wavelength dependence above 4.5 km (the extinction values being the same in the UV and visible wavelength) where the scattering is due to the larger particles in a cloud.

Figure 2. Example of Raman lidar optical extinction profiles at 284, 530 and 607 nm on September 17, 1997, at Hesperia, CA during SCOS97 [21].

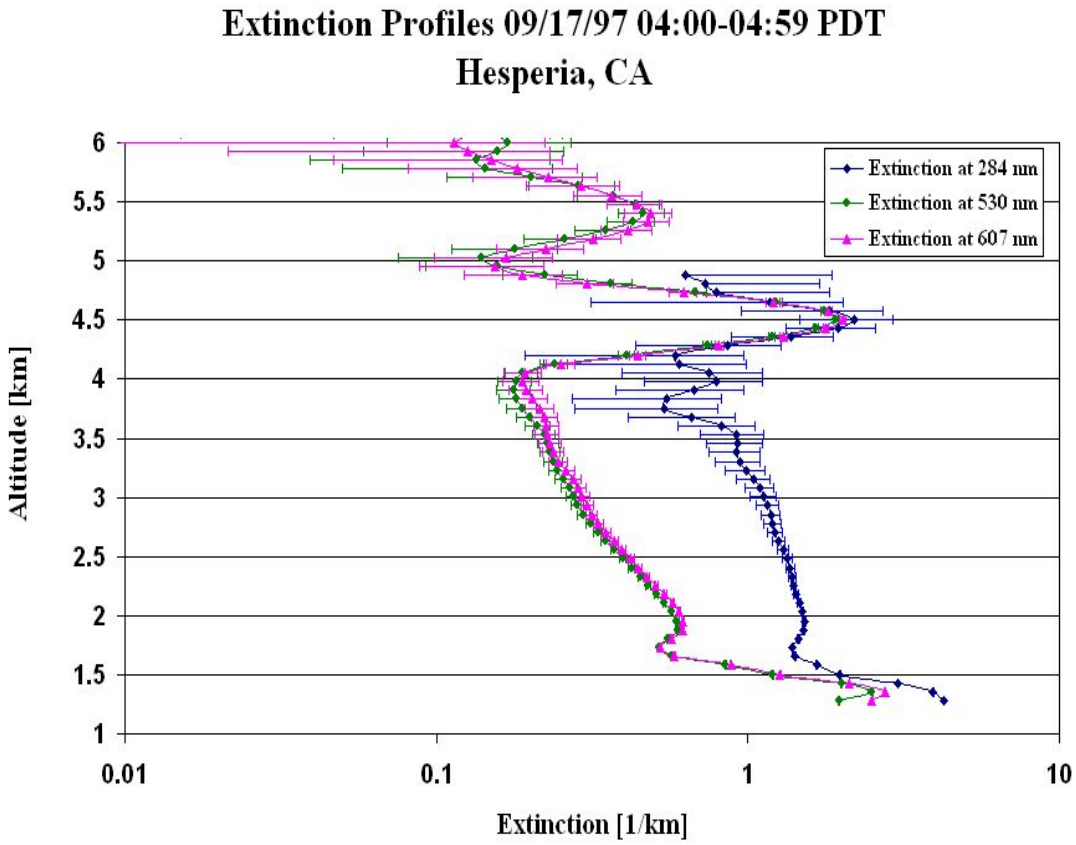

Cloud data obtained using the LAPS Raman lidar during several campaigns are analyzed using the extinction ratios measured at the UV and visible wavelengths to study particle size variations. An example data set from the NARTSO-NEOPS campaign is discussed below. Figure 3 shows the time sequence plots of extinction at the ultraviolet and visible wavelengths on the night of 16 August, 1999 site during the NARSTO-NEOPS campaign in Philadelphia. The vertical profile data is collected in one-minute intervals and a five minute smoothing filter is used to prepare these plots. The extinction data can be compared with simultaneous measurements of the water vapor mixing ratio in Figure 4. During this time period we observe that several aerosol cloud layers advect through the laser beam and our analysis of the ratio of the extinction coefficient of 530/284 shows changes in particle size relative to variations in regions both inside, and surrounding the cloud layers. We also observe high water vapor concentrations in and around the cloud regions in Figure 4.

Figure 3. Time sequence plot of extinction on August 16, 1999 at **(a)** 284nm **(b)** 530nm (the visible wavelength is only available after sunset).

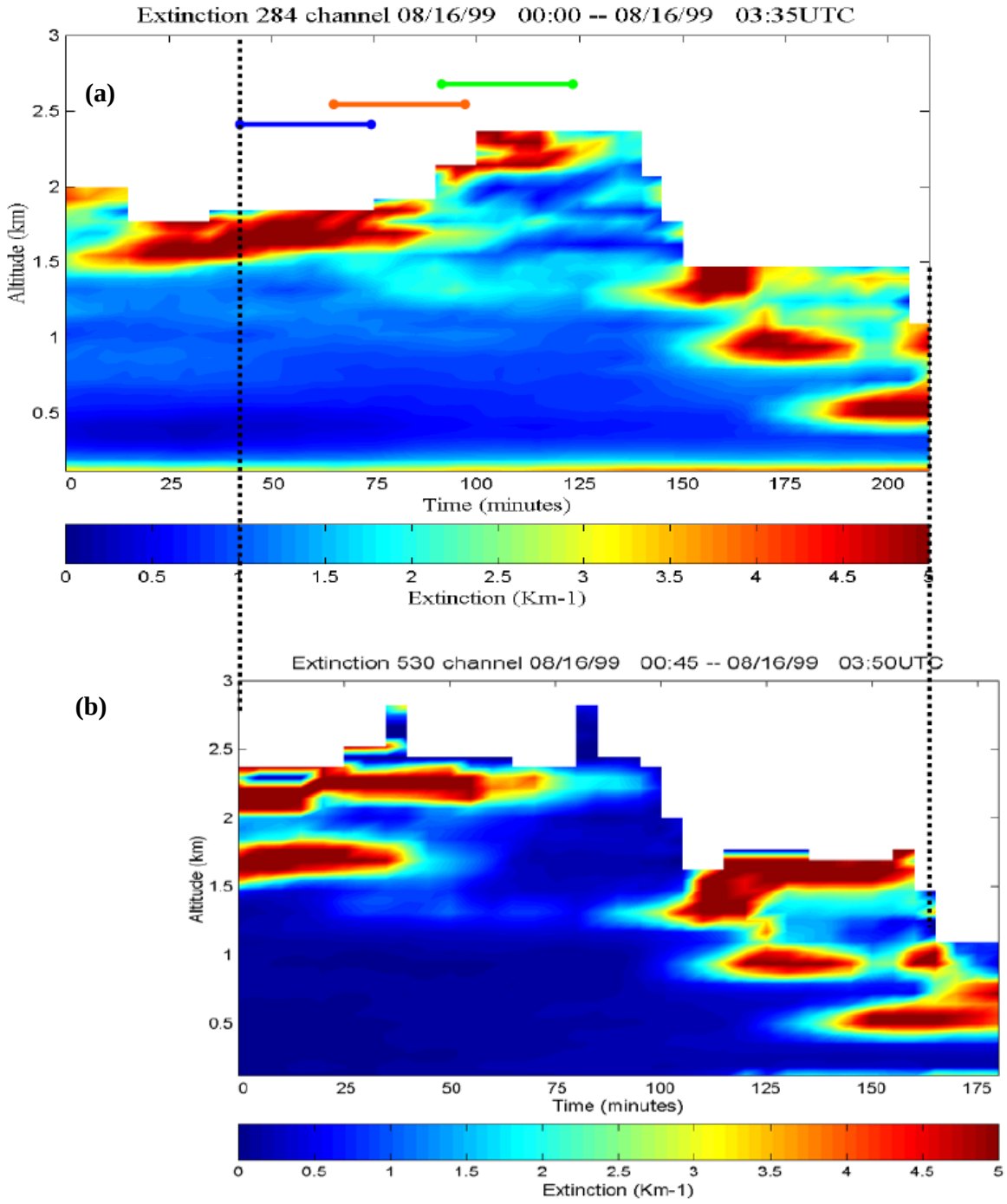

Figure 4. Time sequence plot of water vapor mixing ratio on August 16, 1999.

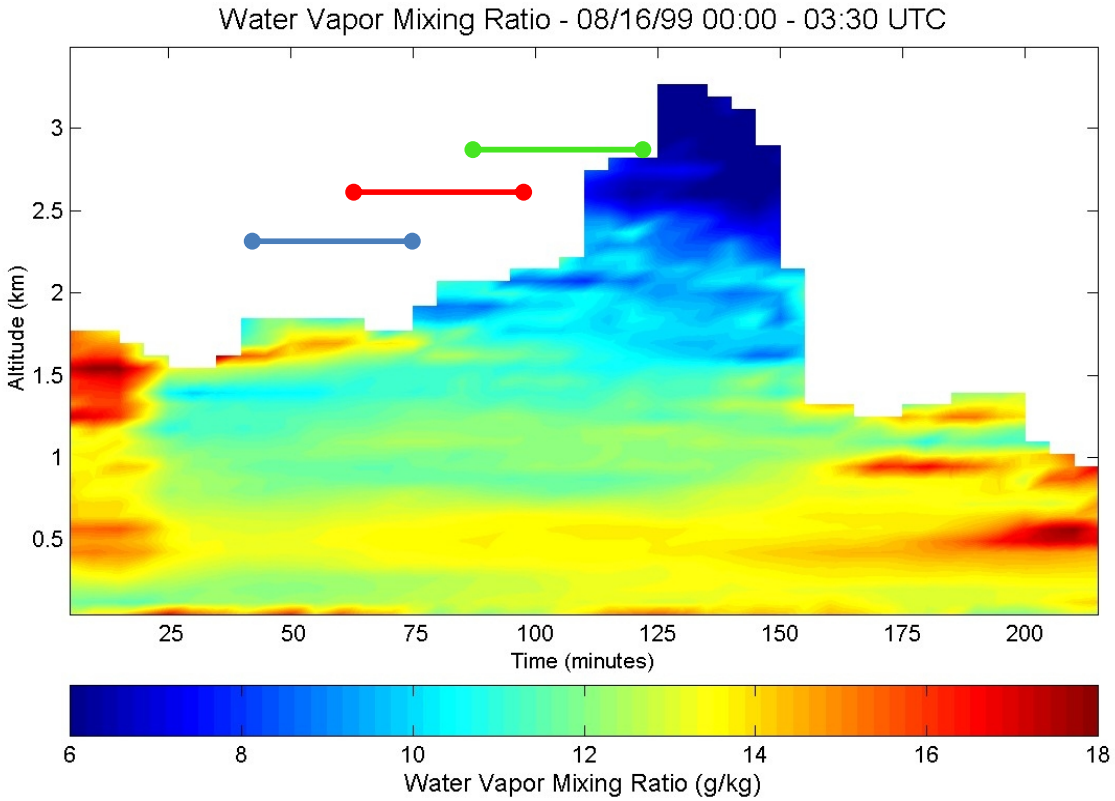

Time sequences of the ratio of the extinction coefficients, as the clouds pass though the laser beam, are shown in Figure 5. Vertical profiles of the extinction ratio are examined in half-hour intervals to observe the mean profile changes and the range of variations during the time sequence. Profiles for the half hour periods are shown in Figure 6 and the three time periods are indicated by the colored lines in Figures 3-5. The time sequence plot showing the ratio of the extinction coefficients enables us to see particle size variation over longer time periods as the overlying atmospheric region changes. We observe particle size variations as both smaller and larger particles pass through the lidar beam. Figure 5 shows regions where particles increase in size (200-800 m), based on the increasing two-wavelength particle extinction ratio, and other regions where the extinction ratio decreases indicates particle sizes decreasing (1.5-2 km). An increase in the 530/284 ratio corresponds to an increase in the relative size of the particles present in the scattering volume. The increasing particles size ratio could indicate regions when the lidar beam passes through the edge of a developing cloud, and into the cloud itself. If the region is sufficiently stable and the lidar beam probes the same region for a significant time, this increasing ratio would indicate particles growing in size due to particles accumulating water vapor or by coagulation of small particles. Similarly a decreasing ratio could indicate passing from inside a cloud to its trailing edge, or a region where the loss of water from aerosol particles results in decreasing size as the cloud is dissipating. A better description of growth and dissipation needs an extended interval of measuring the same volume, possibly with a scanning lidar to follow a volume, or by using two spatially separated instruments.

Figure 5. Ratio of extinction coefficients 530 nm/284 nm on August 16, 1999.

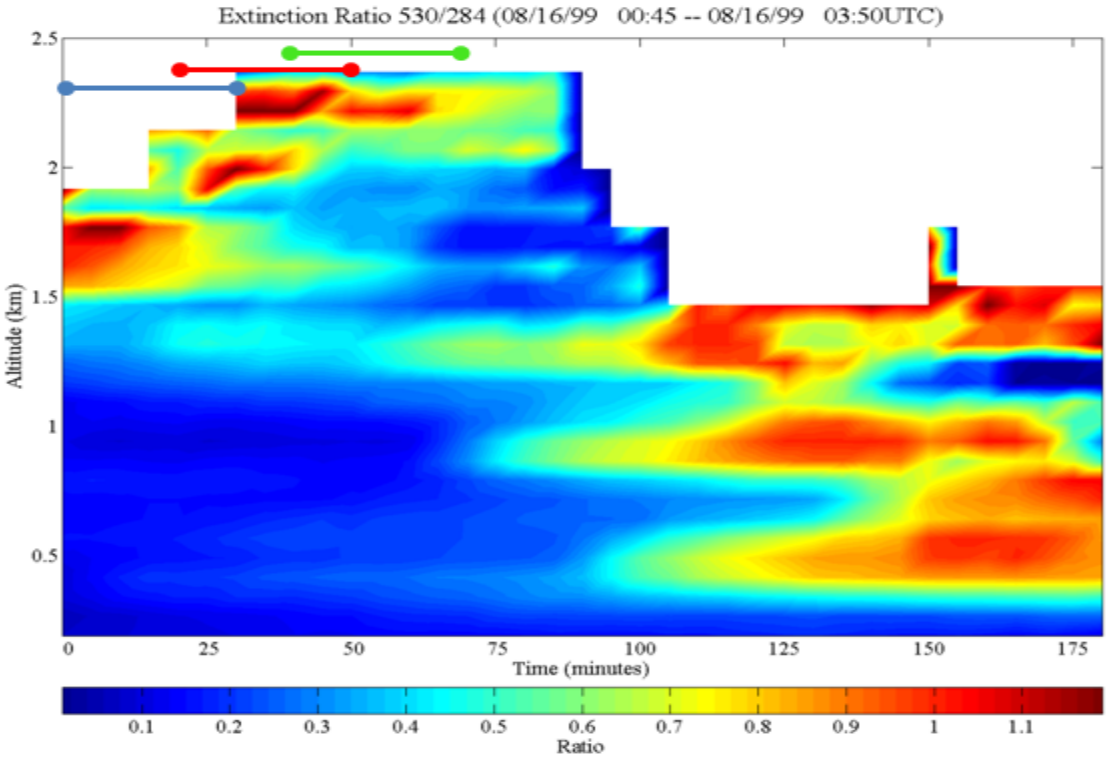

Figure 6. Ratio of extinction coefficient of 530 nm to 284 nm on August 16, 1999 (refer to Figures 3 and 5 to compare variations during the 30 min integrated time periods).

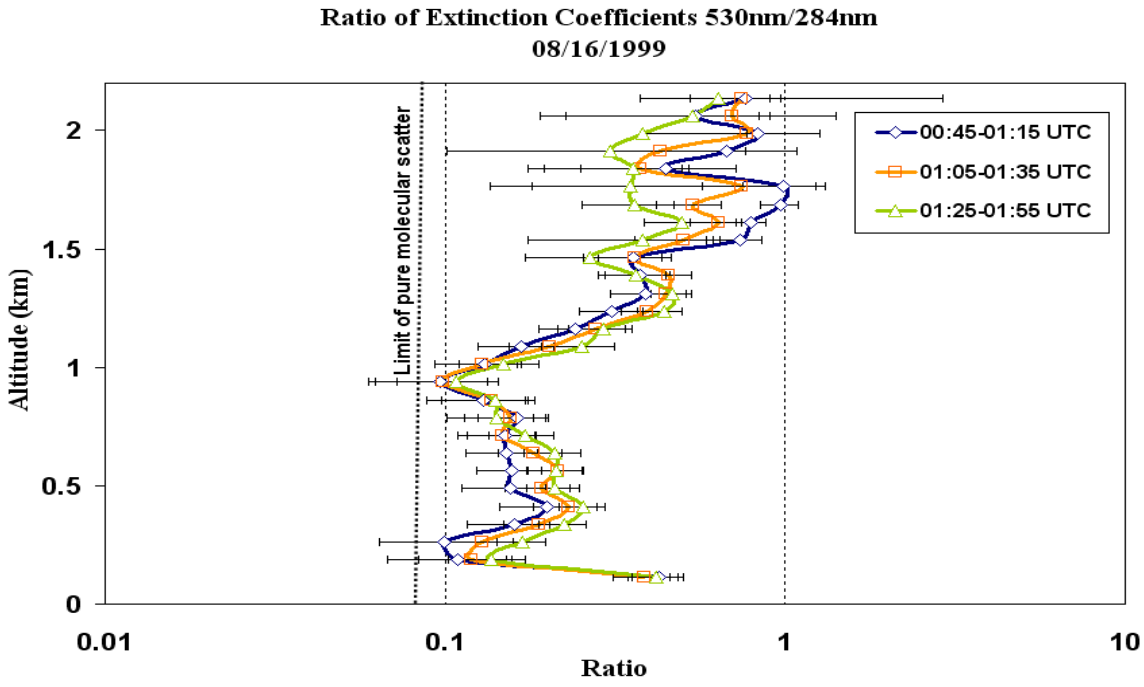

Figures 3(a) and 3(b) show the presence of a cloud at 0045 UTC, between 1.5 km and 2 km, and we observe large extinction coefficient ratios in Figure 6. The ratio is very close to 1.0 for regions inside the cloud and this suggests that the cloud is largely composed of particle sizes much greater than 1 μm. The ratio of 530 nm to 284 nm is also high near the ground (~0.5), indicating a higher concentration of larger aerosol particles in the surface layer. The ratio of the extinction coefficients at these different times (see Figure 6) depicts the evolution of the cloud, as it advects past the laser beam. We see by comparing the time sequences with the ratio plot that as the cloud particle sizes reduce, the ratio falls to lower values. This could be due to the edge of the cloud passing the lidar beam, or the process of dissipation of the cloud. Both conditions are associated with changes from larger to smaller sizes. We can also infer an increase in particle sizes between 1 km and 1.3 km in Figure 6 and the time sequence plots show increasing extinction in that region. Figure 3 also shows the capability of the LAPS Raman lidar to look through moderately thick clouds. This is advantageous because it enables us to study the regions above and below cloud layers.

This dataset provides an opportunity to study the relationship between particle size increase/decrease in cloud regions, in terms of the extinction coefficients, and also changes in relative humidity. Figure 7 shows thirty minute integrated vertical profiles of the extinction coefficients calculated using the LAPS lidar. The three time periods shown correspond to the same time periods used in Figures 3-6. The profiles of the extinction coefficients, at the different time periods, are placed side by side to emphasize the information that these plots have with respect to changing particle sizes in a region. Figure 8 shows the thirty minute integrated vertical profiles of the extinction coefficients along with the relative humidity profile measured using the Raman lidar during that time interval. Examination of Figure 7 shows changes in the extinction coefficients distinctly in two layers, one between 0.2 km and 0.8 km, and the other one between 1.5 km and 2 km. In the lower layer, between 0.2 km and 0.8 km, the extinction coefficients at 530 nm and 607 nm increase in values from 0045 UTC to 0155 UTC, while the extinction coefficients at 284 nm remain relatively constant. By looking at the relative humidity values during these time periods, we see that the increase in extinction values at 530 nm and 607 nm correspond to the simultaneous increase in relative humidity in that region. As the relative humidity values increase, the particles begin to grow in size as the water condenses onto the particles, thus causing an increase in the extinction values at 530 nm and 607 nm. We also observe that the change in extinction coefficients at 284 nm, in the lower region, remain relatively constant during the three time periods. This is consistent with what we would expect to see when the extinction values at longer wavelengths are affected more than at shorter wavelengths as the particles grow in size. As the larger particles form and their population increases in a region, the extinction coefficient values of the longer wavelengths approach those of the shorter wavelengths. Figure 9 shows the ratio of extinction coefficient of 530 nm to 284 nm, and relative humidity profiles measured using the Raman lidar on August 16, 1999 during two selected 30 min integrated time periods. Since a change in the extinction ratio corresponds to a change in the particle size, examination of Figure 9 shows the important relationship between relative humidity and particle size. As the particles grow under the influence of increasing relative humidity, the condensation of water on the particles increases the optical extinction, and the longer wavelength extinction increases more.

Figure 7. Integrated 30 min vertical profiles of optical extinction at 284 nm, 530 nm and 607 nm for time periods shown in Figures 4-9.

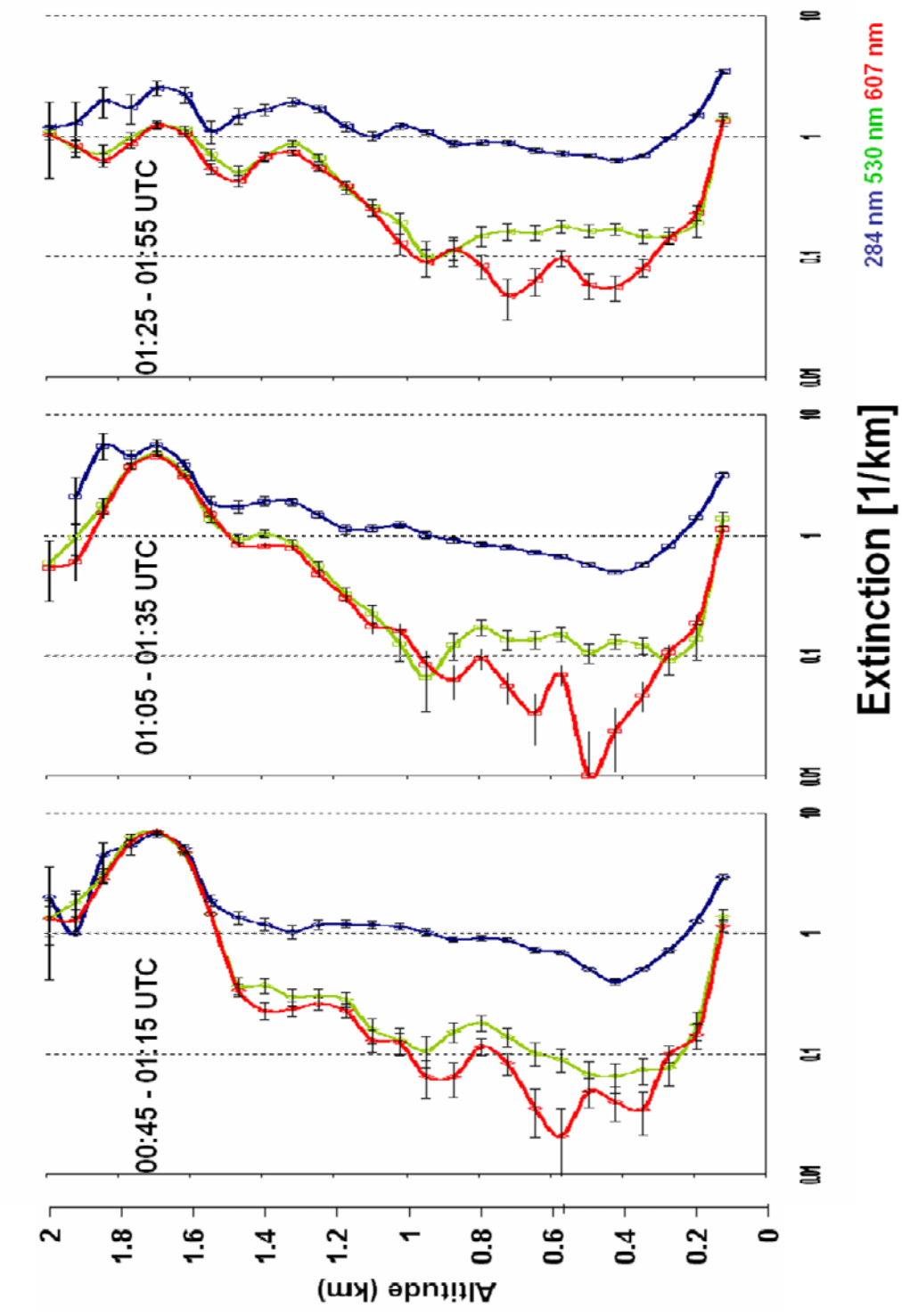

Figure 8. Integrated 30 min vertical profiles of optical extinction at 284 nm, 530 nm and 607 nm and relative humidity calculated using the LAPS lidar water vapor and temperature profiles on August 16, 1999 at **(a)** 0045 UTC **(b)** 0105 UTC.

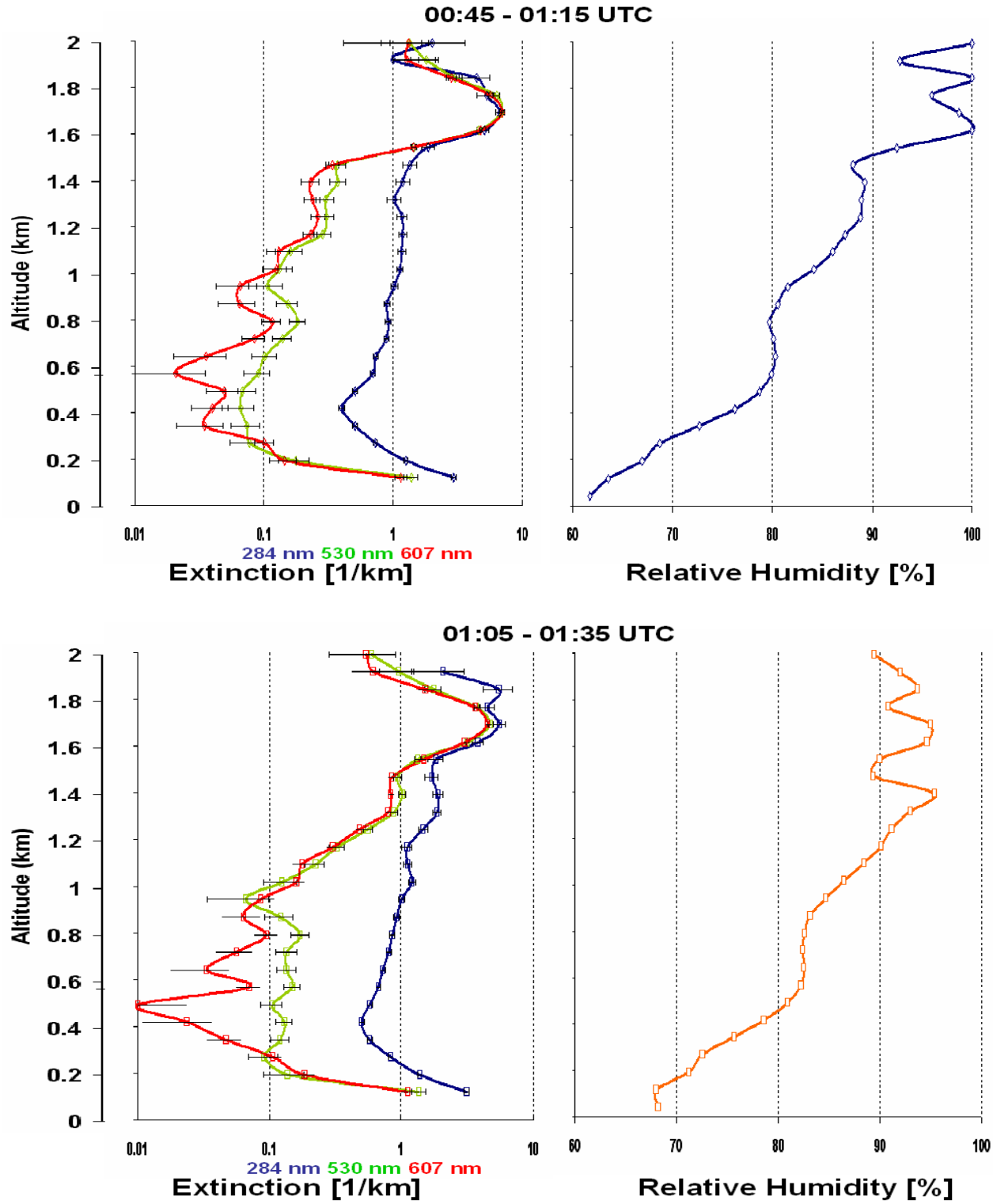

Figure 9. Ratio of extinction coefficient of 530 nm to 284 nm, and relative humidity profiles on August 16, 1999 (30 min integrated time periods). The changing relative humidity correlates with changes in the ratios of the extinction coefficients.

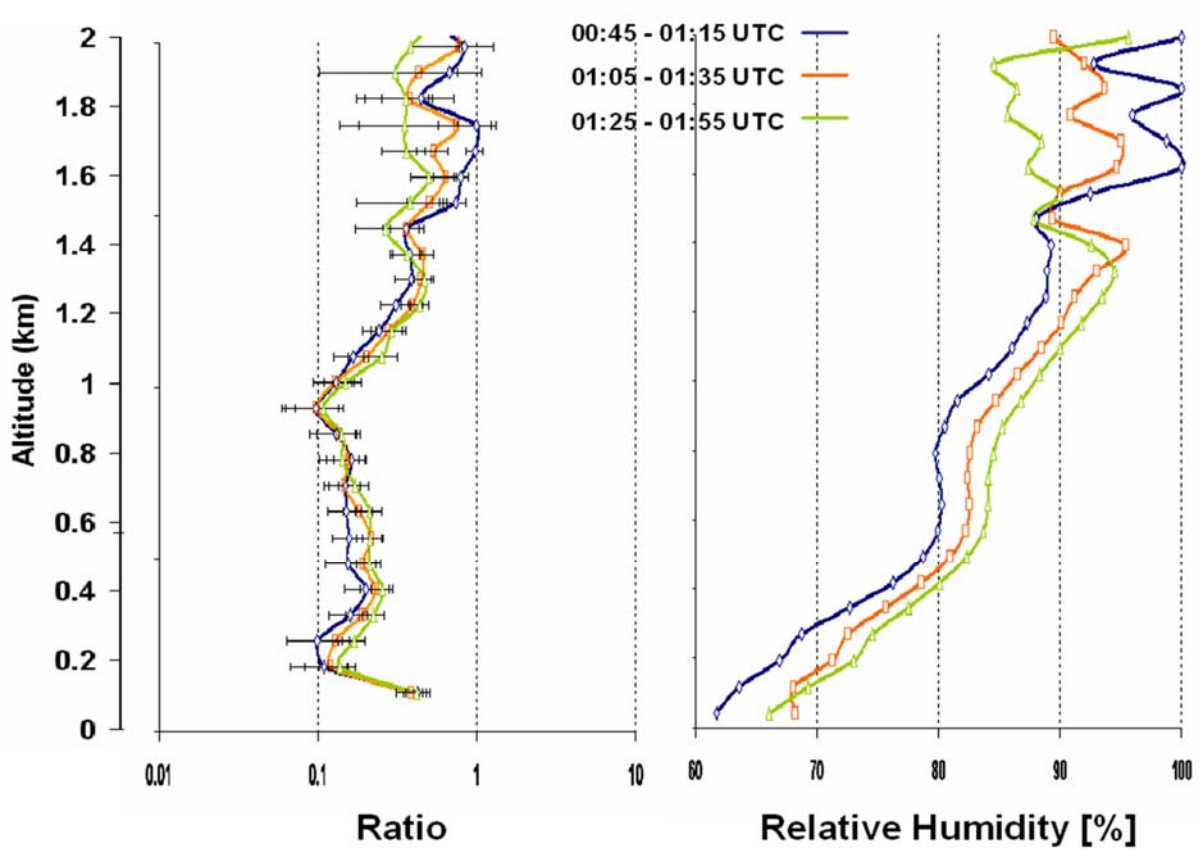

In the upper region, between 1.5 km and 2 km, we observe the presence of a cloud at 0045 UTC, and we see the corresponding extinction ratio reach a value of 1 inside the cloud indicating a distribution of larger particles (>1 μm). Figure 8a and Figure 9 also show that the relative humidity in that region is near 100%. As we examine later times, the cloud particle sizes begin to decrease, the ratio begins to fall to lower values, and the relative humidity decreases in the region. The region becomes populated with a distribution of smaller particle sizes due to the lower relative humidity in the region. The distribution of smaller particles results in the extinction ratio falling to lower values as the extinction coefficient values of the longer wavelengths reduce. The shorter wavelength extinction coefficients are less affected. Notice that the extinction coefficients of the longer wavelengths decrease relative to the shorter wavelengths as the cloud begins to dissipate (see Figure 7).

Figures 8 and 9 clearly exhibit the relationship that exists between the relative humidity, extinction ratio and particle size change. This data set demonstrates that as the relative humidity values increase in a region the particles grow in size due to the water condensing onto the particles, and result in an increase in the extinction ratio. Similarly, when the relative humidity in the region becomes less, the resulting distribution of smaller particles leads to a drop in the extinction ratio.

4. Conclusions

Raman lidar techniques provide profiles of aerosol and cloud properties by simultaneously measuring optical extinction profiles at several different wavelengths. We demonstrate the capability of this technique by using the multi-wavelength extinction profiles obtained from the LAPS Raman lidar compared with simulations of extinction ratios based upon Mie calculations, to study particle size variations. The ratio of the extinction coefficients describes the size dependence for most of the accumulation mode particles (size range from 0.1 to 2 μm) and size independence for particles much larger than the scattering wavelength. We see that the analysis of the ratios provide a means to describe changes in the size distribution of aerosols in the atmosphere and leads to a capability to describe formation and dissipation processes in cloud layers. The multi-wavelength extinction profiles are used along with relative humidity, from Raman lidar profiles of water vapor and temperature, to observe the evolution of cloud structures. As particles grow in size from water condensation, the extinction and the visible/ultraviolet extinction ratio measurements show increases with increasing relative humidity. Similarly, we find that when the relative humidity in the region decreases, the resulting distribution of smaller particles leads to a drop in the magnitude of the extinction ratio. In order to improve quantitative measurements and better understand the size variations within a volume, it will be necessary to follow an air parcel. A tracking lidar could track an air parcel from upwind to downwind locations. The ability of Raman lidar to obtain the multi-wavelength extinction profiles simultaneously with the water vapor and temperature profiles provides an opportunity to construct useful models and better understand the cloud physics processes.

Acknowledgments

Most of this work was performed when the authors were located at Penn State University and they acknowledge their appreciation for the opportunities and colleagues there. The work reported here builds upon the dissertations, theses, and papers of several previous graduate students and post-doctoral researchers of the Penn State University Lidar Laboratory. Credit is given particularly to T.D. Stephens, P.T. Haris, F. Balsiger, M.D. O'Brien, S. Rajan, S.L. Mathur, K.R. Mulik, S.T. Esposito, E.J. Novitsky, and G. Li for the work that they accomplished.

References and Notes

1. Arya, S.P. *Air Pollution Meteorology and Dispersion*, Oxford University Press, Oxford, 1999.
2. Intergovernmental Panel on Climate Change, *Climate Change 2001: The Scientific Basis: Contribution of Working Group I to the Third Assessment Report of the Intergovernmental Panel on Climate Change (Climate Change 2001)*, J. T. Houghton, Y. Ding, D. J. Griggs, M. Noguer, P. J. van der Linden, X. Dai, K. Maskell, C. A. Johnson, Eds., Cambridge University Press, Cambridge, U.K. (2001).
3. Twomey, S. The influence of pollution on the shortwave albedo of clouds, *J. Atmos. Sci.* **1977**, 34, 1149-1152.
4. Albrecht, B.A. Aerosols, cloud microphysics, and fractional cloudiness, *Science* **1989**, 245, 1227-1230.

5. Wielick, B.A., Cess, R.D., King, M.D., Randall, D.A., and Harrison, E.F. Mission to planet Earth: Role of clouds and radiation in climate, *Bull. Amer. Meteorol. Soc.* **1995**, 76, 2125-2153.
6. Gillespie, J.B., Ligon, D.A., Pellegrino, P.M., Fell Jr, N.F., and Wood, N.J. Development of a broadband lidar system for remote determination of aerosol size distributions, *Meas. Sci. Technol.* **2002**, 13, 383-390.
7. Philbrick, C.R. Raman lidar measurements of atmospheric properties, *Atmospheric Propagation and Remote Sensing III* **1994**, SPIE 2222, 922-931.
8. Philbrick, C.R. Overview of Raman lidar techniques for air pollution measurements, in *Lidar Remote Sensing for Industry and Environment Monitoring II,* **2002**, SPIE 4484, 136 – 150.
9. Ansmann, M.A., Muller, D., Wandinger, U. and Althausen, D. Multi-year aerosol observations with dual-wavelength Raman lidar in the framework of EARLINET, *Geophys. Res. Letts.*, **2004**, 109, D13203.
10. Ansmann, A., Mattis, I., Müller, D., Wandinger, U., Althausen, D., and Damoah, R. Ice formation in Saharan dust over Europe observed with temperature/humidity/aerosol Raman lidar, *J. Geophys. Res.* **2005**, 110, D18S12.
11. Novitsky, E.J. and Philbrick, C.R. Multistatic lidar profiling of urban atmospheric aerosols, *J. Geophys. Res.-Atmos*, **2005**, 110, DO7S11.
12. Measures, R.M. *Laser Remote Sensing*, Wiley-Interscience, NewYork, 1984.
13. Rajan, S., Kane, T.J., and Philbrick, C.R. Multiple wavelength Raman lidar measurements of atmospheric water vapor, *Geophy. Res. Let.* **1994**, 21, 2499-2502.
14. Balsiger, F., and Philbrick, C.R. Comparison of lidar water vapor measurements using Raman scatter at 266 nm and 532 nm, *Application of Lidar to Current Atmospheric Topics* **1996**, SPIE 2833, 231-240.
15. O'Brien, M.D. Stevens, T.D., Balsiger, F. and Philbrick, C.R. Optical extinction from Raman lidar measurements, *Optical Instruments for Weather Forecasting* **1996**, SPIE 2832, 45-52.
16. Balsiger, F., Haris, P.T., and Philbrick, C.R. Lower tropospheric temperature measurements using a rotational Raman lidar, *Optical Instruments for Weather Forecasting* **1996**, SPIE 2832, 53–60.
17. Esposito, S.T. *Applications and Analysis of Raman Lidar Techniques for Measurements of Ozone and Water Vapor in the Troposphere*, Master of Science Thesis for Penn State University, Department of Electrical Engineering, 1999.
18. Mulik, K.R., and Philbrick, C.R. Raman lidar measurements of ozone during pollution events, in Advances in Laser Remote Sensing **2001**, 20th ILRC 2000, 443-446.
19. Stevens, T.D. *Bistatic Lidar Measurements of Lower Troposphere Aerosols*, Doctoral Dissertation at Penn State University, Department of Electrical Engineering, 1996.
20. Boheren, C.F. and Huffman, D.R. *Absorption and Scattering of Light by Small Particles*, John Wiley & Sons, Inc., USA, 1983.
21. Li, G. and Philbrick, C.R. Lidar measurements of airborne particulate matter, *Lidar Remote Sensing for Industry and Environment Monitoring III* **2003**, SPIE 4893, 93-104.